SOME FLUID FLOW CHARACTERISTICS OF A CROSS FLOW TYPE HYDRAULIC TURBINE

W. W. Durgin
Mechanical Engineering Department
Worcester Polytechnic Institute
Worcester, Massachusetts

W. K. Fay
Hoyle, Tanner and Associates, Inc.
Londonderry, New Hampshire

ABSTRACT

A small cross-flow type hydraulic turbine was designed to allow investigation of the internal hydrodynamics. Testing of this machine revealed that significant flow was carried within the runner and thus did not contribute to second stage power production. The theory of cross-flow turbines was modified to account for the portion of flow entrained in the runner. The remainder of the flow was assumed to cross-flow to the second stage through the central region of the machine. It was observed that such cross-flow does not exist in the form of a well defined jet as is usually assumed. Both existing theory and modified theory were compared to measured performance data.

INTRODUCTION

In recent years increased concern over the rising cost of fossil fuel has prompted the reactivation of many lowhead hydroelectric plants. Currently, the feasibility of rebuilding these sites hinges on the availability of inexpensive turbines. One of the more easily constructed and least expensive turbines, the cross-flow type, is surrounded by controversy. This turbine is ideal for small, run-of-the-river operations, because it's efficiency is much less dependent on flow rate than other types of machines. Unfortunately, cross-flow turbines are being shunned by many lowhead hydro entrepreneurs because of their reputed low efficiencies. Maximum efficiencies of 68% (1), 73% (2), 60% (3), 50% (4), and 84% (5) have been cited in the literature.

A.G.M. Mitchell invented the cross-flow turbine around 1900 (6). Banki, in a series of papers from 1916 to 1918, presented his theory of operation and the results of his experiments. He indicated that efficiencies of 80% were attainable. (7) However, his data and experimental procedures are not available. In 1949, Mockmore and Merryfield "freely translated" and expanded upon Banki's analyses. They constructed a model turbine and presented a formal paper comparing their machine's performance to the expanded analysis. The 68% experimentally attained efficiency was well below the 87.8% predicted. Mockmore and Merryfield's machine differed from Banki's in the design of the inlet nozzle. Banki's machine had a nozzle which was close coupled to the runner casing, thus the entrance pressure was not necessarily equal to atmospheric pressure. Mockmore and Merryfield's nozzle discharged into the runner at atmospheric pressure.

The Ossberger Turbinen Fabrik of West Germany commercially manufactures cross-flow turbines. They have claimed efficiencies of 84%. In 1982, Johnson and White, constructed and tested a model turbine. They attained efficiencies, "generally in the range of 60% to 70%"(3).

The objective of the present experiment was to determine specific flow characteristics of a cross-flow turbine. A small machine was constructed with a plexiglas pressure casing and an open ended runner supported on a cantilever shaft. The open end allowed the flow patterns inside the runner to be analyzed with both stroboscopic and photographic techniques. The open end allowed objects to be placed inside the rotating runner to alter the internal flow patterns. The nozzle was designed so the effects of varying the admittance arc could be examined. The turbine was instrumented and the data obtained was used to construct turbine characteristic curves. The reduced data in conjunction with the stroboscopic and photographic evidence were used to analyze and modify the prevailing cross-flow theory.

An attempt was made to measure the cross-flow by extraction in order to determine the percent of flow retained in the blading. A pipe with a slot was inserted inside the rotating runner to intercept the flow which was collected and measured. The technique worked well at partial loads, however, each time loads nearing the point of maximum efficiency were applied, the extraction pipe would deflect and interfere with the runner. Enough data was obtained at partial loads to allow extrapolation of the extracted flow rate at full load.

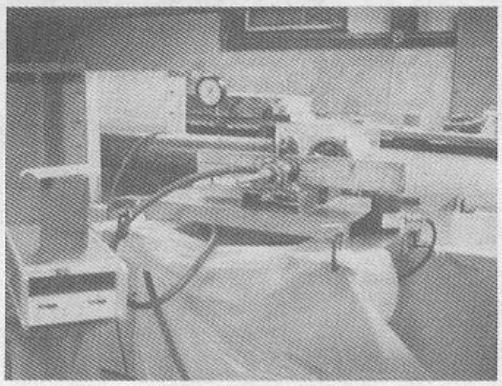

Fig. 1 Test Set-up, Dynamometer Side

NOMENCLATURE

c - Entrance nozzle loss coefficient
H - Turbine Head
g - Acceleration of gravity
Q - Volumetric flow rate
R_1 - Runner outside radius
R_2 - Runner inside radius
s - Admittance arc length
T - Torque
U - Peripheral wheel velocity
V - Absolute velocity
v - Relative velocity
x - ratio of entrained flow to total flow
η - Hydraulic efficiency
ϕ - Speed ratio
ρ - Fluid density
σ - Admittance arc angle
ψ - Loss factor
1 - Stage entrance
4 - Stage exit
' - Indicates exit of cross flow
" - Indicates exit of entrained flow

EXPERIMENTAL EQUIPMENT & TEST PROCEDURES

Preliminary Setup and Instrumentation

The model was secured to the test flume in the Student Laboratory at Alden Research Laboratory of Worcester Polytechnic Institute. The Student Laboratory was equipped with a penstock drawing from a pond and terminating at a surge tank. A 12 inch secondary line from the tank with a standard 12 x 6 cast iron venturi meter was connected through a gate valve to the machine which discharged into a flume. The flow meter was equipped with a manometer to determine differential pressure.

Two dynamometers, a nine inch Alden absorption dynamometer and a Prony friction brake were utilized for power measurements. Because of their individual characteristics, the Alden machine was used up to ϕ = 0.5 with the Prony serving the higher range.

Two methods of recording runner shaft speed were used. A hand held, flyball type tachometer was used for speeds over 200 rpm. Speeds under 200 rpm were determined with a hand held revolution counter and a laboratory stop clock. The turbine inlet pressure was recorded with a bourdon test gauge.

Photographs were taken with a camera and a stroboscopic light, set so that the camera's shutter triggered the high intensity stroboscope.

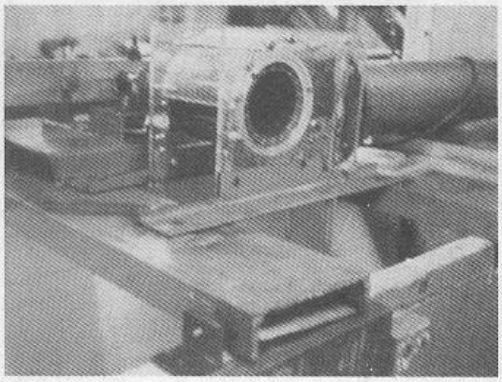

Fig. 2 Test Set-up, Viewing-port Side

Standard Test Procedure

For a given test configuration, the gate valve in the entrance line was opened to provide a predetermined deflection of the venturi meter manometer. Data from the manometer, bourdon gauge, tachometer and load cell monitor were recorded so the torque was adjusted by predetermined increments. This procedure was repeated until the desired range of machine performance was complete.

The procedure outlined above, was used to collect data to construct the turbine characteristic curves. Tests to determine the optimum admittance arc for maximum efficiency required moving the guide vane in small increments. This was accomplished by removing the side casing, moving the vane, reinstalling the side and realigning the casing.

This procedure was repeated for each guide vane position.

In order to intercept the interstage flow, a scoop was fabricated from a piece of three-inch pipe and was inserted into the runner, through the port hole, and fixed to the casing. The same procedure was used to obtain the data.

RESULTS

The most significant results were the observation of the high percentage of flow entrained inside the runner blades and the modification of the existing theory of operation to account for the entrained flow.

Internal Flow Patterns

The stroboscope revealed the theoretically predicted free standing jet did not exist inside the runner. A percentage of the total inflow entering the runner did cross inside the runner from a number of blade passages. These flows combined to from a poorly defined jet. The jet crossed through the runner and entered the second stage with a high degree of incidence losses. The remaining percentage of the flow entering the first stage became entrained in the runner blades and was flung tangentially from the runner at the draft tube entrance.

Two general trends were observed. First, as the runner speed was varied from zero to maximum, the entrained fluid flow varied from zero to a maximum and as the speed was similarly varied, the cross flow went from 100% of the total flow to zero cross flow. Secondly, as the admittance arc was varied from 35° to 80°, the entrained flow increased from zero to full entrainment.

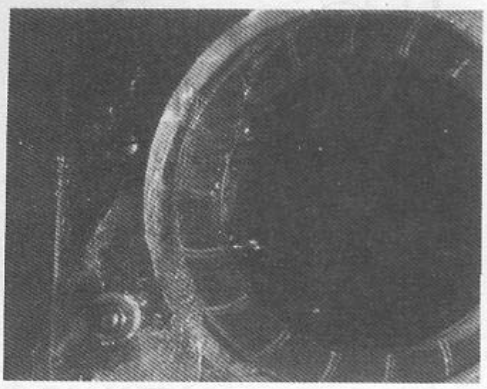

Fig. 3 Viewing Port, camera 90° to runner negligable cross flow runner
$\phi = 0.97, \eta = 4\%$

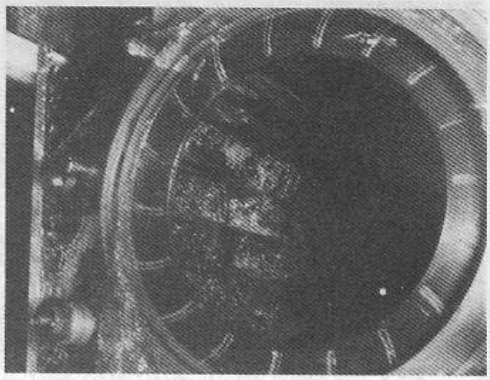

Fig. 4 Viewing port, camera angled to runner, runner buckets nearly empty
$\phi = 0.97, \eta = 4\%$

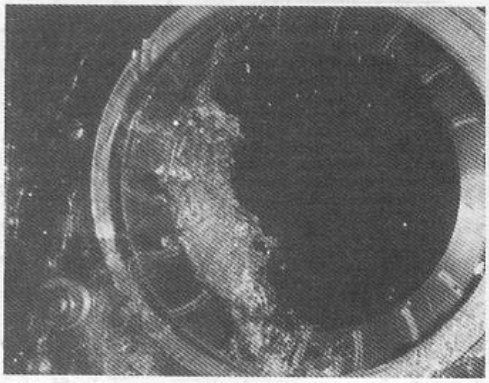

Fig. 5 Viewing port, camera 90° to runner, major cross flow
$\phi = 0.48, \eta = 61\%$

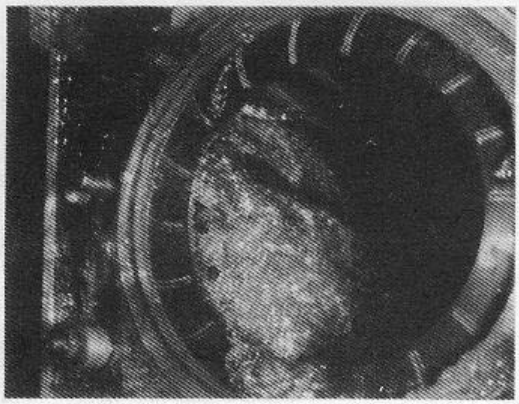

Fig. 6 Viewing port, camera angled to runner buckets full
$\phi = 0.48$, $\eta = 61\%$

Cross Flow Extraction

Cross flow extraction data was obtained in the range $0.62 \leq \phi \leq 1.0$. When $\phi = 0.62$ the extraction scoop deflected against the rotating runner thus, interfering with machine operation. Extrapolation to $\phi = 0.5$ indicated a maximum efficiency of approximately 42% would have been attained with the cross flow eliminated. Performance data collected concurrently for the configuration, but without the flow extracted indicated a 51% max efficiency. The second stage thus, contributed approximately 17% to the overall model performance, Fig. 7.

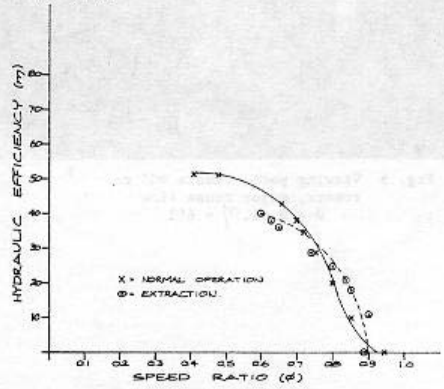

Fig. 7 Performance comparison of normal operation and operation with the second stage flow extracted

Efficiencies

The maximum efficiency attained by the model was 61% and occurred when the speed ratio was 0.48, Fig. 8. The variation in maximum efficiency versus the admittance arc angle is shown in Fig. 9. As the admittance arc angle was increased, the nozzle cross sectional area increased thus allowing more water to enter the machine. The efficiency increased to a maximum of 61% as the admittance angle was increased to 63 degrees. At admittance angles greater than 63 degrees, the maximum efficiency decreased.

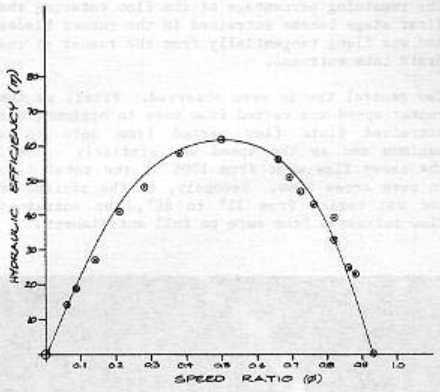

Fig. 8 Graph of efficiency versus speed ratio for the experimental data

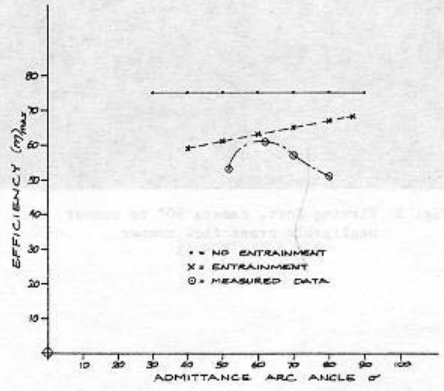

Fig. 9 Graph of maximum efficiency versus jet admission arc for experiment and theory

DISCUSSION

The existing theory for the operation of the cross-flow turbine was altered to account for the percentage of flow entrained in the runner. The efficiency predicted with the modified theory is closer to the observed efficiency. The existing theory predicted a maximum efficiency of 87% while the modified theory predicted an efficiency of 66% indicating that entrained flow must be accounted for in predictive techniques.

Fluid can be entrained in the runner once it is sufficiently slowed in radial velocity that centripetal acceleration dominates. Both boundary layer friction and lack of pressure relief at the nozzle trailing edge cause deceleration. Once flow is entrained in the runner, the performance is clearly affected as some of the power cannot be extracted from the entrained flow.

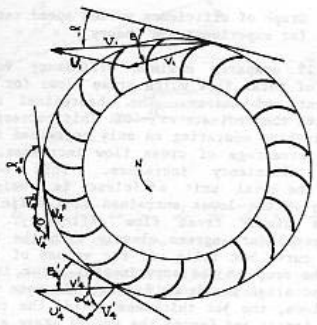

Fig. 10 Notation

Using the notation shown in figure ten, the tangential velocities are:

(1) $Vt_1 = V_1 \cos\alpha_1$

(2) $Vt_4' = V_4' \cos\alpha_4'$

(3) $Vt_4'' = V_4'' \cos\alpha_4''$

Where station 1 is the inlet, station prime is the exit for fluid which cross flows, and station is the exit for fluid which has been entrained in the runner. Considering a control volume about the outer radius, ri, of the runner and assuming uniformity of the respective velocities on the entrance and exit areas, the torque can be written.

(4) $T=\rho Q_t R_1 V_{t1} + \rho Q_j R_1 V_{t4}' + \rho Q_e R_1 V_{t4}''$

letting

(5) $Q_e = XQ_t$

and

(6) $Q_j = (1-x)Qt$

then

(7) $T=\rho Q_j R_1 (V_{t4}' + V_{t1}) + \rho Q_e R_1 (V_{t4}'' + V_{t1})$

the power can be evaluated using

(8) $P=TW = TU_1/R_1$

or

(9) $P=\rho Q_t U_1 (1-x)(V_4' \cos\alpha_4' + V_1\cos\alpha_1) + X(V_4''\cos\alpha_4'' + V_1\cos\alpha_1)$

Assuming that $\alpha_4'' = \Pi$ so that the entrained flow is flung tangentially off the runner with $V_4'' = U_1$ together with the velocity relationships.

(10) $V_1 \cos\alpha_1 = v_1 \cos\beta_1 + U_1$

(11) $V_4' \cos\alpha_4' = v_4' \cos\beta_1 + U_1$

and a factor to account for blade and internal losses

(12) $V_4 = \psi V_1$

then

(13) $P=\rho Q_t U_1 (1-x)(1+\psi)(V_1\cos\alpha_1 - U_1) + X(V_1\cos\alpha_1 - U_1)$

Defining the velocity ration as

(14) $\phi = U_1/V_1$

the power is

(15) $P=\rho Q_t V_1^2 \phi (1-x)(1+\psi)(\cos\alpha_1 - \phi) + X(\cos\alpha_1 - \phi)$ The maximum theoretical power is

(16) $P_{th} = \rho Q_t gH$

(17) $= \rho Q_t \frac{V_1^2}{2C^2}$

Where

(18) $V_1 = C\sqrt{2gH}$

The efficiency becomes $\eta = P/P_{th}$ or

(19) $\eta = 2C^2 \phi (\cos\alpha_1 - \phi)\left((1-x)(1+\psi) + X\right)$

with the maximum at

(20) $\phi = \frac{1}{2}\cos\alpha_1$ for η max

This is the same ratio as for a cross-flow turbine without entrainment. The maximum efficiency is, then,

$$(21)\ \eta_{max} = \tfrac{1}{2}C^2 \cos^2\alpha_1 \left((1-x)(1+\psi) + X\right)$$

The efficiency can be split into parts corresponding to the cross-flow and entrained power transfers as

$$(22)\ \eta = (1-x)\eta_J + X\eta_E$$

$$(23)\ \eta_J = 2C^2 \phi\ (\cos\alpha_1 - \phi)\ (1+\psi)$$

and

$$(24)\ \eta_e = 2C^2\phi(\cos\alpha_1 - \phi)$$

There is a maximum amount of entrained flow which can be carried by the runner which depends on the particular geometry of the runner and the velocity ratio. If S is the admittance arc length

then

$$(25)\ X_{max} = \frac{1}{2}\frac{R_1}{S}\frac{\phi}{\sin\alpha}\left(1 - \left(\frac{R_2}{R_1}\right)^2\right)$$

The degradation of efficiency is thus entrainment limited by this reduction.

Figure 11 compares efficiency versus velocity ratio for both experiment and theory. The two theoretical curves representing operation with and without entrained flow were predicted by assuming typical model operating parameters. The parameters were α=16°, ψ=0.8 C=0.95, a 60° admittance arc and a 0.75 bucket fill ratio. The theoretical curves bracket the experimental data for ϕ=0.6. Below ϕ=0.6 the data falls below but close to the theoretical curves. It is interesting to note that as the runner operates on larger amounts of entrained flow the point of maximum efficiency shifts to lower values of ϕ.

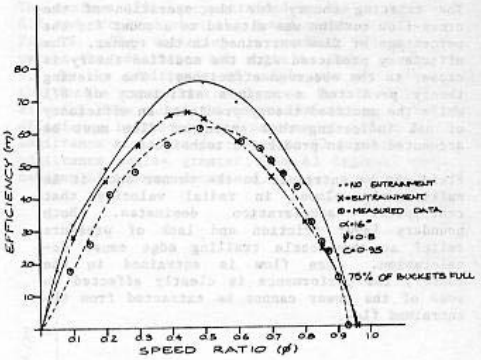

Fig. 11 Graph of efficiency versus speed ratio for experiment and theory

Figure 12 compares maximum efficiency versus percent of total flow which cross flows for both experiment and theory. The theoretical curve intersects the ordinate at η=40%. This corresponds to the turbine operating on only entrained flow. As the percentage of cross flow increases, the maximum efficiency increases. This occurs because the total unit efficiency is a weighted function of the lower entrained flow efficiency and the higher cross flow efficiency. The experimental data agrees closely with the theoretical curve but falls off for values of (1-x) 0.5. The drop of the experimental curve is due to second stage incidence losses. As more water cross-flows, the jet thickness inside the runner becomes larger and forces the second stage abso-

lute inlet angle to increase. When the angle increases beyond the design value off peak operation results.

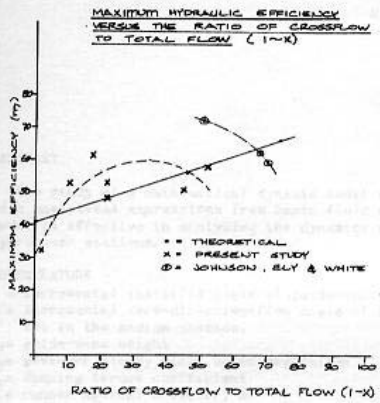

Fig. 12 Maximum hydraulic efficiency versus the ratio of cross flow to total flow (1-X)

Summary

A model cross flow turbine was constructed in a configuration to allow extraction of the inter-stage cross flow and observation of the runner's internal flow patterns.

The maximum efficiency attained was 61%.

It was determined the second stage contributes approximately 17% of the power.

It was discovered that a significant amount of entrained flow was carried by the runner, and did not cross to the second stage. An analysis was developed which incorporated the effects of entrained flow. This analysis was matched to the measured efficiency data using reasonable values of ψ, C, and % blade fill. The efficiency predicted with the modified theory is closer to the observed efficiency. The existing theory predicted a maximum efficiency of 87% while the modified theory predicted an efficiency of 66% indicating that entrained flow must be accounted for in predictive techniques.

REFERENCES

1. Mockmore, C.A., and Merryfield, F., "The Banki Water Turbine," Engineering Experimental Station Bulletin #25, February 1949, p. 22.

2. Balji, D.E., Turbomachines: A Guide To Design, Selection and Theory, John Wiley and Sons, New York, N.Y. 1981, p. 333.

3. White, Frank, Johnson, William and Ely, Richard, "Design and Testing of an Inexpensive Cross-Flow Turbine" Transactions ASME Small Hydropower Machinery, 1982 p. 129.

4. Conversation with George Balalau of Energy Research and Applications Institute, Santa Monica, California.

5. Ossberger Turbinerfabrik sales literature

6. Haimerl, L.A., "The Cross-Flow Turbine," Water Power Engineering Magazine, I.P.C. Business Press, New York, N.Y. January 1960 issue, p.5.

7. Banki, Von Donat, "Eine neue Wasserturbine," Feitschrift Des Vereines Deutcher Ingenieure, Berlin, Germany, 3 August 1918 issue, p. 515.

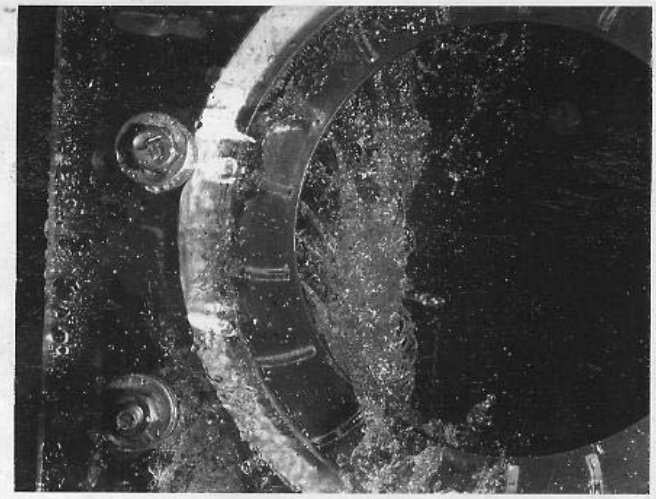

N = 350 RPM

Q = .761 CFS

Photograph No. 1 - Original Nozzle

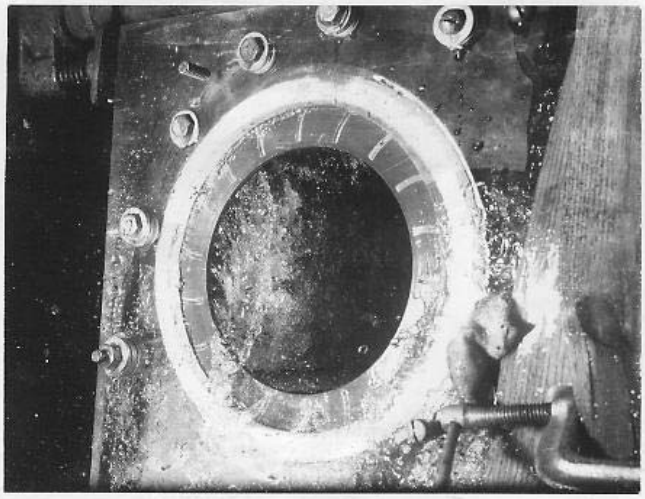

N = 350 RPM

Q = .761 CFS

Photograph No. 2 - Original Nozzle

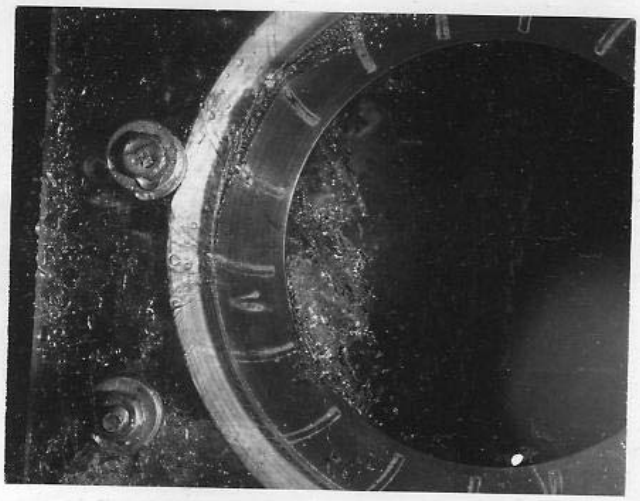

N = 550 RPM

Q = .747 CFS

Photograph No. 3 - Original Nozzle

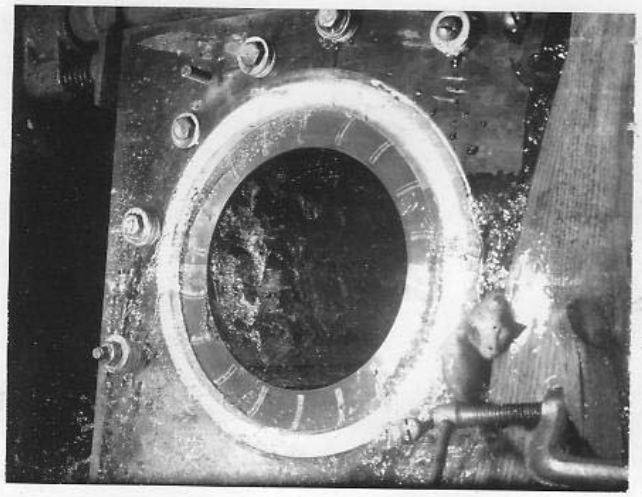

N = 550 RPM

Q = .747 CFS

Photograph No. 4 - Original Nozzle

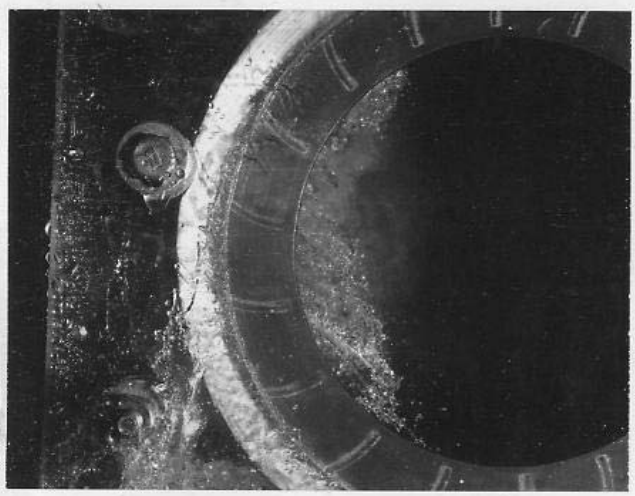

N = 700 RPM

Q = .762 CFS

Photograph No. 5 - Original Nozzel

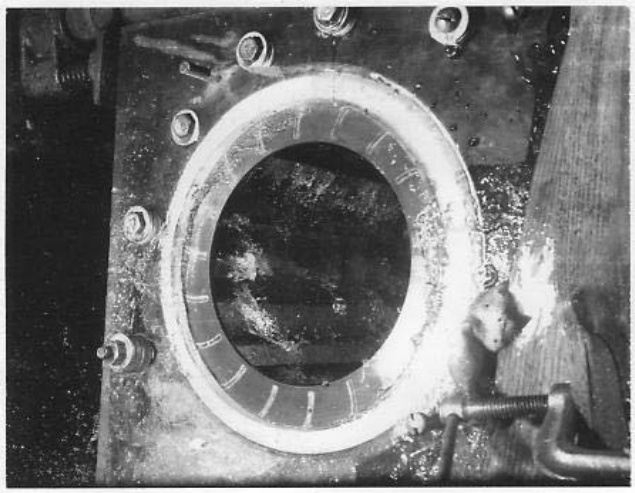

Photograph No. 6 - Original Nozzel

N=350 RPM

Q=0.761 CFS

Photograph No. 7 - Original Nozzle taken without flash

N= 350 RPM

Q= 0.761 CFS

Photograph No. 8- Draft Tube Flow

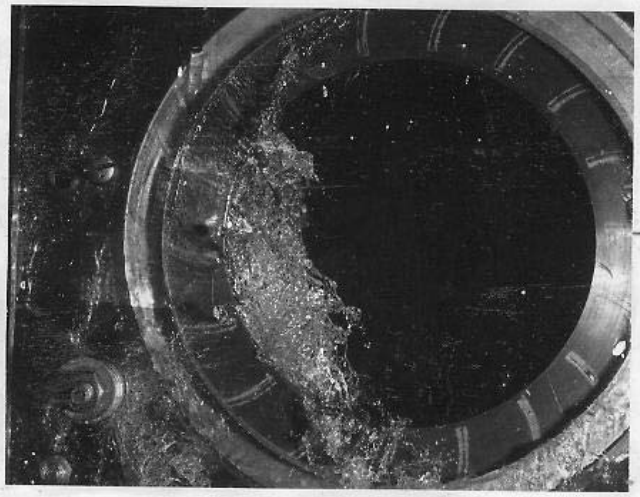

N = 350 RPM

Q = 0.477 CFS

Photograph No. 9 - Modified Nozzle

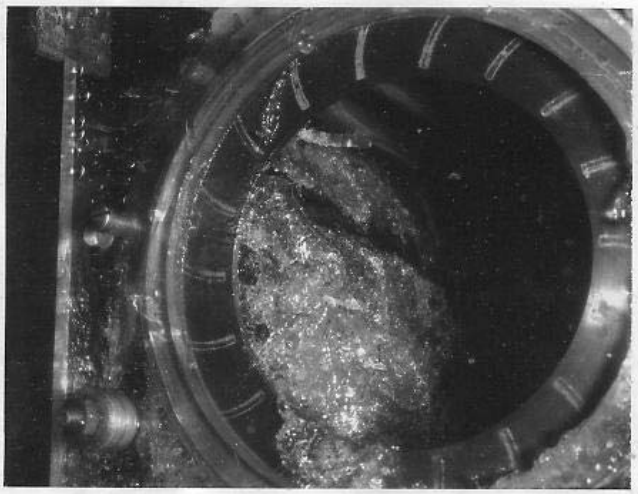

N = 350 RPM

Q = 0.477 CFS

Photograph No. 10 - Modified Nozzle

old mill Road

-869-2118 -
after 6:30 PM

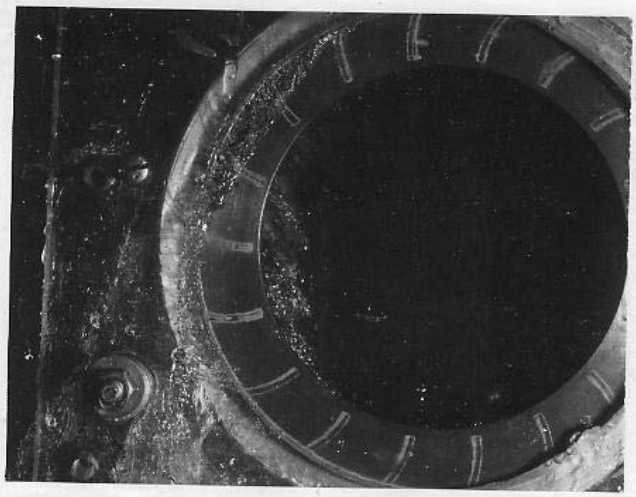

N = 550 RPM

Q = .472 CFS

Photograph 11 - Modified Nozzle

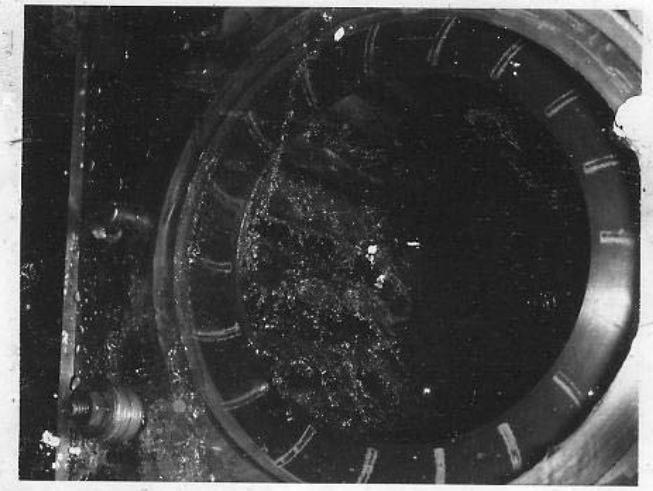

N = 550 RPM

Q = 1472 CFS

Photograph 12 - Modified Nozzle

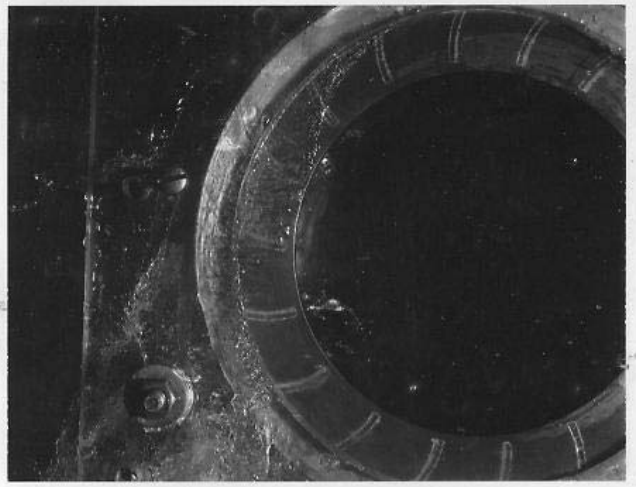

N = 690 RPM

Q = .476 CFS

Photograph No. 13 - Modified Nozzle

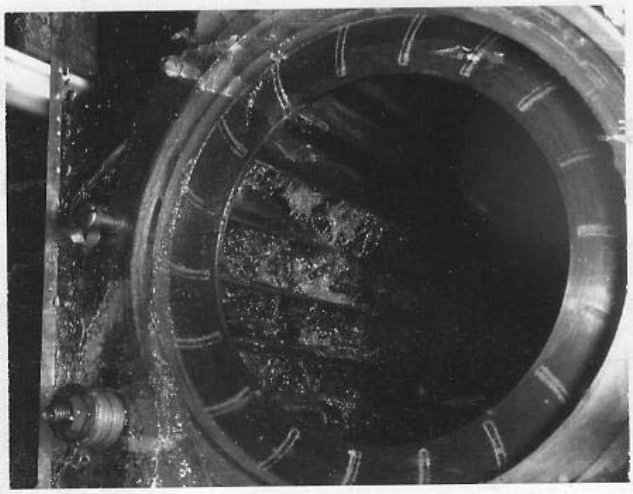

N = 690 RPM

Q = .476 CFS

Photograph No. 14 - Modified Nozzle

N = 400 RPM

Q = 0.428 CFS

Photograph No. 15 - Runner operating without cross-flow

N = 400 RPM

Q = 0.428 CFS

Photograph No. 16 - Close-up view of above Draft tube

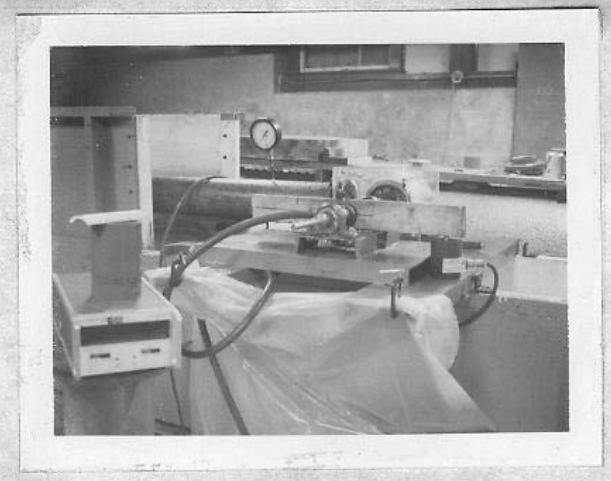

Photograph No. 17 - Test Set-up, Dynamometer side

Photograph No. 18 - Test Set-up, Viewing port side

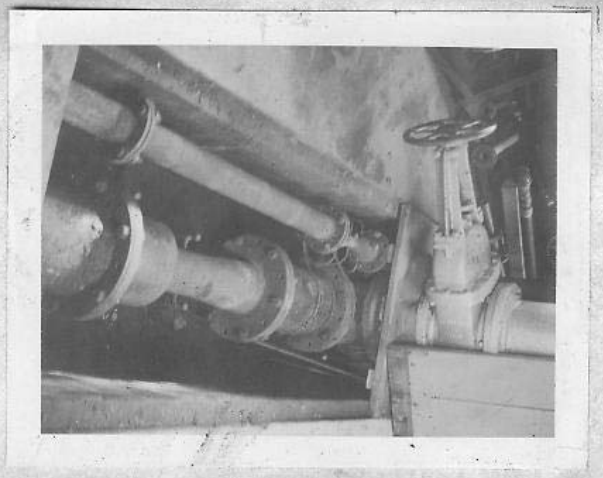

Photograph No. 19 - Venturi Meter and Flow Control Valve

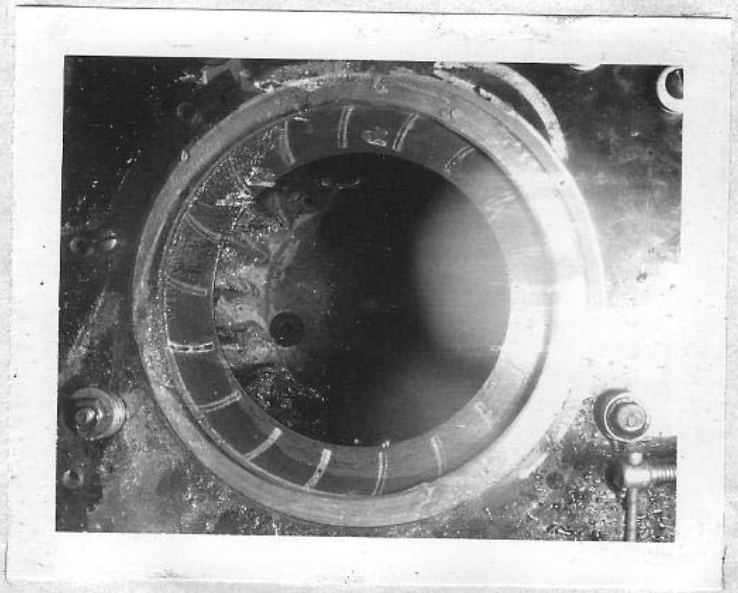

Photograph No. 20 - Installation of PVC Sector